

Magnon bands in twisted bilayer honeycomb quantum magnets

Xingchuan Zhu(朱兴川), Huaiming Guo(郭怀明), and Shiping Feng(冯世平)
Citation: Chin. Phys. B, 2021, 30 (**7**): 077505. DOI: 10.1088/1674-1056/abeee5
Journal homepage: http://cpb.iphy.ac.cn; http://iopscience.iop.org/cpb

What follows is a list of articles you may be interested in

Emergent O(4) symmetry at the phase transition from plaquette-singlet to antiferromagnetic order in quasi-two-dimensional quantum magnets

Guangyu Sun(孙光宇), Nvsen Ma(马女森), Bowen Zhao(赵博文), Anders W. Sandvik, and Zi Yang Meng(孟子杨)
Chin. Phys. B, 2021, 30 (**6**): 067505. DOI: 10.1088/1674-1056/abf3b8

Electric-field-induced in-plane effective 90° magnetization rotation in Co_2FeAl/PMN-PT structure

Cai Zhou(周偲), Dengyu Zhu(朱登玉), Fufu Liu(刘福福), Cunfang Feng(冯存芳), Mingfang Zhang(张铭芳), Lei Ding(丁磊), Mingyao Xu(许明耀), and Shengxiang Wang(汪胜祥)
Chin. Phys. B, 2021, 30 (**5**): 057504. DOI: 10.1088/1674-1056/abd7de

Influence of the anisotropy on the magneto-acoustic response of magnetic surface acoustic wave resonators

Yawei Lu(鲁亚巍), Wenbin Hu(胡文彬), Wan Liu(刘婉), Feiming Bai(白飞明)
Chin. Phys. B, 2020, 29 (**6**): 067504. DOI: 10.1088/1674-1056/ab8375

Three- and two-dimensional calculations for the interface anisotropy dependence of magnetic properties of exchange-spring $Nd_2Fe_{14}B/\alpha$-Fe multilayers with out-of-plane easy axes

Qian Zhao(赵倩), Xin-Xin He(何鑫鑫), Francois-Jacques Morvan(李文瀚), Guo-Ping Zhao(赵国平), Zhu-Bai Li(李柱柏)
Chin. Phys. B, 2020, 29 (**3**): 037501. DOI: 10.1088/1674-1056/ab69e9

Model of output characteristics of giant magnetoresistance (GMR) multilayer sensor

Jiao-Feng Zhang(张教凤), Zheng-Hong Qian(钱正洪), Hua-Chen Zhu(朱华辰), Ru Bai(白茹), Jian-Guo Zhu(朱建国)
Chin. Phys. B, 2019, 28 (**8**): 087501. DOI: 10.1088/1674-1056/28/8/087501

SPECIAL TOPIC — Twistronics

Magnon bands in twisted bilayer honeycomb quantum magnets*

Xingchuan Zhu(朱兴川)[1], Huaiming Guo(郭怀明)[2,†], and Shiping Feng(冯世平)[1]

[1] *Department of Physics, Beijing Normal University, Beijing* 100875, *China*

[2] *Key Laboratory of Micro-Nano Measurement-Manipulation and Physics (Ministry of Education), Department of Physics, Beihang University, Beijing* 100191, *China*

(Received 21 January 2021; revised manuscript received 10 March 2021; accepted manuscript online 16 March 2021)

We study the magnon bands of twisted bilayer honeycomb quantum magnets using linear spin wave theory. Although the interlayer coupling can be ferromagnetic or antiferromagnetic, we keep the intralayer one ferromagnetic to avoid possible frustration. For the interlayer ferromagnetic case, we find the magnon bands have similar features with the corresponding electronic energy spectrums. Although the linear dispersions near the Dirac points are preserved in the magnon bands of twisted bilayer magnets, their slopes are reduced with the decrease of the twist angles. On the other hand, the interlayer antiferromagnetic couplings generate quite different magnon spectra. The two single-layered magnon spectra are usually decoupled due to the opposite orientations of the spins in the two layers. We also develop a low-energy continuous theory for very small twist angles, which has been verified to fit well with the exact tight-binding calculations. Our results may be experimentally observed due to the rapid progress in two-dimensional magnetic materials.

Keywords: magnon bands, twisted bilayer, quantum magnets, linear spin wave theory

PACS: 75.70.Cn, 75.75.–c, 75.30.Ds, 71.70.Gm **DOI:** 10.1088/1674-1056/abeee5

1. Introduction

The recent discovery of the correlated insulator and unconventional superconductivity in twisted bilayer graphene has attracted intense interests.[1–8] By rotating the layers to a small angle, a misalignment induced in the bilayer system introduces a long-period moiré superlattice. Such a superlattice therefore modulates the electronic structure, and leads to nearly flat band at the magic angles. These bands become so narrow that the electron-electron correlations dominate over kinetic energy, giving rise to the above correlated quantum phases.[9] Since twisted bilayer graphene is relatively simple and highly tunable, it is anticipated that this system can serve as an ideal platform to investigate the strongly-correlated physics.

Moiré superlattices have also been employed to engineer flat bands in other two-dimensional (2D) materials, such as twisted double-bilayer graphene, trilayer graphene, and twisted bilayer of the transition metal dichalcogenide, where rich correlation phenomena have been revealed.[10–19] While research has been primarily centered on twisted electronic systems, there appear theoretical studies addressing the remarkable physical properties in twisted Kitaev bilayers[20] and twisted optical lattices.[21,22] It is accepting that twisting is a simple and general approach to creating exotic quantum matter.

Recently rapid progress in 2D magnetic atomic crystals has been made.[23–27] Various monolayer and multilayer van der Waals (vdW) magnetic materials have been discoveried, and different kinds of ferromagnetic (FM) and antiferromagnetic (AFM) orders have been observed.[28–36] The 2D vdW magnetic materials have a huge potential to create novel functional devices, and have important applications in the next-generation nanoelectronics.[37–42] Of course, they are also important in fundamental research. The physics can be described by a generalized Heisenberg spin Hamiltonian, and a broad range of parameter regimes can be realized in a rich variety of materials. All three spin Hamiltonians, *i.e.*, Ising, XY, and Heisenberg models, can be recovered in specific limits.[43–46] Besides, external perturbations, such as gating, strain, *etc*., can further tune the range of model parameters.[47–51] These make the magnetic 2D materials into an ideal platform to examine the well-established theories[52–54] and explore new quantum phases.[55–57]

*Project supported by the National Natural Science Foundation of China (Grant Nos. 11774019, 11974051, and 11734002), the Fundamental Research Funds for the Central Universities and the HPC Resources at Beihang University, and the National Key Research and Development Program of China (Grant No. 2016YFA0300304).

†Corresponding author. E-mail: hmguo@buaa.edu.cn

© 2021 Chinese Physical Society and IOP Publishing Ltd

Motivated by these advances in the studies of the twisted 2D materials and 2D magnetic materials, we study how the twist alters the magnon bands in twisted bilayer honeycomb quantum magnets here. We keep the intralayer FM coupling, and study the magnon bands with interlayer FM and AFM couplings in AA(AB)-stacked and twisted bilayer quantum magnets. Our study is closely related to the rapid experimental progress in two-dimensional magnetic materials.

2. AA-stacked honeycomb magnets

Twisted bilayers are characterized by non-zero angle θ between two honeycomb layers. Since the twist may be performed based on AA-stacked bilayer, we start from the spin-1/2 Heisenberg model on this geometry, which can be written as

$$H = -J\sum_{\langle ij\rangle,\ell} \boldsymbol{S}_{i,\ell}\cdot\boldsymbol{S}_{j,\ell} - J_\perp \sum_{\langle ij\rangle} \boldsymbol{S}_{i,2}\cdot\boldsymbol{S}_{j,1}, \tag{1}$$

where $\boldsymbol{S}_{i,\ell} = (S^x_{i,\ell}, S^y_{i,\ell}, S^z_{i,\ell})$ is the spin-1/2 operator at site i in layer $\ell = 1,2$; the summation runs over nearest-neighbor sites $\langle ij\rangle$; J ($J_\perp$) is the intralayer (interlayer) coupling constant, and we first consider the FM case, *i.e.*, $J>0$ and $J_\perp>0$.

Using Holstein–Primakoff (HP) transformation, the spin operators are expressed in term of bosonic creation and annihilation operators. In the FM case, the transformation in the linear spin-wave theory is defined as

$$S^+_i = \sqrt{2S}a_i, \quad S^z_i = S - a^\dagger_i a_i. \tag{2}$$

After ignoring a constant and four-operator terms, the resulting bosonic tight binding Hamiltonian becomes

$$\begin{aligned} H^{\rm AA}_{\rm FM} =& -J\sum_{\langle ij\rangle,\ell}\frac{1}{2}(a^\dagger_{i,\ell}a_{j,\ell} + a_{i,\ell}a^\dagger_{j,\ell}) \\ & -J_\perp\sum_i \frac{1}{2}(a^\dagger_{i,1}a_{i,2} + a_{i,1}a^\dagger_{i,2}) \\ & +\frac{3J+J_\perp}{2}\sum_{i,\ell} a^\dagger_{i,\ell}a_{i,\ell}. \end{aligned} \tag{3}$$

Performing a Fourier transformation, the above Hamiltonian writes as $H = \sum_{\boldsymbol{k}} \psi^\dagger_{\boldsymbol{k}}\mathcal{H}_{\rm FM}(\boldsymbol{k})\psi_{\boldsymbol{k}}$, where

$$\psi_{\boldsymbol{k}} = \{a_{A,1}(\boldsymbol{k}), a_{B,1}(\boldsymbol{k}), a_{A,2}(\boldsymbol{k}), a_{B,2}(\boldsymbol{k})\}^{\rm T}$$

is the basis, and

$$\mathcal{H}^{\rm AA}_{\rm FM}(\boldsymbol{k}) = \mathcal{H}^{\rm AA}_0(\boldsymbol{k}) + \frac{3J+J_\perp}{2}, \tag{4}$$

with

$$\mathcal{H}^{\rm AA}_0(\boldsymbol{k}) = \begin{pmatrix} 0 & f(\boldsymbol{k}) & -J_\perp/2 & 0 \\ f^*(\boldsymbol{k}) & 0 & 0 & -J_\perp/2 \\ -J_\perp/2 & 0 & 0 & f(\boldsymbol{k}) \\ 0 & -J_\perp/2 & f^*(\boldsymbol{k}) & 0 \end{pmatrix}, \tag{5}$$

and $f(\boldsymbol{k}) = -(J/2)(1 + {\rm e}^{-{\rm i}\boldsymbol{k}\cdot\boldsymbol{a}_1} + {\rm e}^{-{\rm i}\boldsymbol{k}\cdot\boldsymbol{a}_2})$ [$\boldsymbol{a}_1 = (\sqrt{3},0), \boldsymbol{a}_2 = (\sqrt{3}/2, 3/2)$ the primitive vectors].

With a unitary transformation $\psi_{\boldsymbol{k}} = U(\boldsymbol{k})\phi_{\boldsymbol{k}}$ ($U(\boldsymbol{k})^\dagger U(\boldsymbol{k}) = \mathbb{I}$), the above Hamiltonian is directly diagonalized, and the spectrum contains four branches: $(3J+J_\perp)/2 \pm J_\perp/2 \pm |f(\boldsymbol{k})|$. The magnon band structure is shown in Fig. 1. Compared to that of single-layer honeycomb magnet, the Dirac points are shifted upward and downward by $J_\perp/2$, which is exactly the same as that of AA-stacked graphene except for an overall translation of $3J+J_\perp/2$.

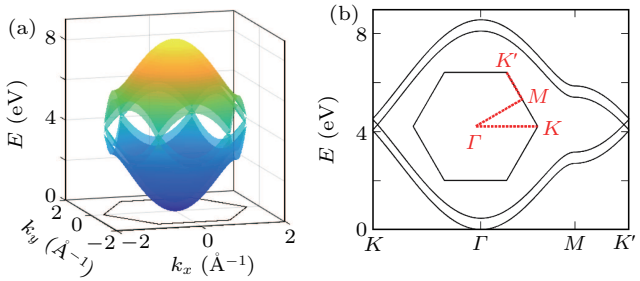


Fig. 1. (a) The magnon band structure of AA-stacked FM bilayer. (b) The magnon bands along the high symmetry points in the first Brillouin zone, which are shown in the inset. The parameter is $J_\perp/J = 0.17$.

Now we turn to consider the case with interlayer AFM exchange, *i.e.*, $J_\perp<0$, while the intralayer coupling remains FM coupling. The following magnetic configuration is assumed: the spins in layer 1 (2) are along the positive (negative) z axis. The HP transformation in layer 1 is the same as that in Eq. (2). In layer 2, the spin is in the opposite direction, thus the spin operators write as

$$S^+_{2,i} = a^\dagger_{i,2}\sqrt{2S}, \quad S^z_{2,i} = a^\dagger_{i,2}a_{i,2} - S. \tag{6}$$

The resulting bosonic tight binding Hamiltonian becomes

$$\begin{aligned} H^{\rm AA}_{\rm AFM} =& -J\sum_{\langle ij\rangle,\ell}\frac{1}{2}(a^\dagger_{i,\ell}a_{j,\ell} + a_{i,\ell}a^\dagger_{j,\ell}) \\ & -J_\perp\sum_i \frac{1}{2}(a_{i,1}a_{i,2} + a^\dagger_{i,1}a^\dagger_{i,2}) \\ & +\frac{3J-J_\perp}{2}\sum_{i,\ell} a^\dagger_{i,\ell}a_{i,\ell}. \end{aligned} \tag{7}$$

Under the basis

$$\psi_{\boldsymbol{k}} = \{a_{\rm A,1}(\boldsymbol{k}), a_{\rm B,1}(\boldsymbol{k}), a^\dagger_{\rm A,2}(-\boldsymbol{k}), a^\dagger_{\rm B,2}(-\boldsymbol{k})\}^{\rm T},$$

the above Hamiltonian in the momentum space can be written as

$$\mathcal{H}^{\rm AA}_{\rm AFM}(\boldsymbol{k}) = \mathcal{H}^{\rm AA}_{0}(\boldsymbol{k}) + \frac{3J - J_\perp}{2}, \quad (J_\perp < 0). \tag{8}$$

We use Bogoliubov transformation $\psi_{\boldsymbol{k}} = U(\boldsymbol{k})\phi_{\boldsymbol{k}}$ to diagonalize the above Hamiltonian

$$U(\boldsymbol{k})^\dagger \mathcal{H}^{\rm AA}_{\rm AFM}(\boldsymbol{k}) U(\boldsymbol{k}) = D,$$

with D is a diagonal matrix. The transformation satisfies $U(\boldsymbol{k})^\dagger s_z U(\boldsymbol{k}) = s_z$ to maintain the commutation relation of bosons. Then we have $s_z \mathcal{H}^{\rm AA}_{\rm AFM}(\boldsymbol{k}) U(\boldsymbol{k}) = U(\boldsymbol{k}) s_z D$, which means the Bogoliubov transformation $U(\boldsymbol{k})$ is the eigenvector of $s_z \mathcal{H}^{\rm AA}_{\rm AFM}$ with the eigenvalue $s_z D$. Thus we obtain the magnon spectrum

$$E^{\pm}_{\boldsymbol{k}} = \sqrt{\left(|f(\boldsymbol{k})| \pm \frac{3J - J_\perp}{2}\right)^2 - \left(\frac{J_\perp}{2}\right)^2},$$

each of which is two-fold degenerate. For small $J_\perp$ and near the Dirac points,

$$E^{\pm}_{\boldsymbol{k}} \sim \pm|f(\boldsymbol{k})| + \frac{3J - J_\perp}{2} - \frac{J_\perp^2}{4(3J - J_\perp)},$$

and the Dirac point is slightly shifted downward, and the dispersion remains linear. As shown in Fig. 2, the magnon spectrum is almost the same as that of the single-layer FM case, suggesting the magnon excitations from different spin alignments are decoupled.

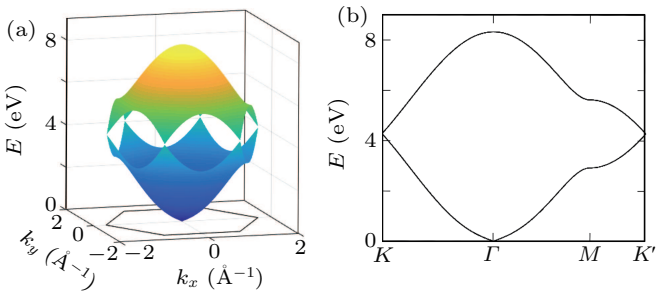


Fig. 2. (a) The magnon band structure of AA-stacked FM bilayer with interlayer AFM exchange. (b) The magnon bands along the high symmetry points in the first Brillouin zone. The parameters are the same as those of Fig. 1.

3. AB-stacked honeycomb magnets

Next we consider AB-stacked bilayer quantum magnets, which can be viewed as rotating AA-stacked bilayer by $\theta = 60^\circ$. In the intralayer and interlayer FM case, the bosonic tight binding Hamiltonian is

$$\begin{aligned} H^{\rm AB}_{\rm FM} = & -J_\perp \sum_i \frac{1}{2}(a^\dagger_{i_{\rm B},1} a_{i_{\rm A},2} + a_{i_{\rm B},1} a^\dagger_{i_{\rm A},2}) \\ & + \frac{J_\perp}{2} \sum_i (a^\dagger_{i_{\rm B},1} a_{i_{\rm B},1} + a^\dagger_{i_{\rm A},2} a_{i_{\rm A},2}) \\ & - J \sum_{\langle ij\rangle,\ell} \frac{1}{2}(a^\dagger_{i,\ell} a_{j,\ell} + a_{i,\ell} a^\dagger_{j,\ell}) \\ & + \frac{3J}{2} \sum_{i,\ell} a^\dagger_{i,\ell} a_{i,\ell}. \end{aligned} \tag{9}$$

In the momentum space, it is written as

$$\mathcal{H}^{\rm AB}_{\rm FM}(\boldsymbol{k}) = \mathcal{H}^{\rm AB}_{0}(\boldsymbol{k}) + \mathcal{D}_{\rm FM}, \tag{10}$$

with

$$\mathcal{H}^{\rm AB}_{0}(\boldsymbol{k}) = \begin{pmatrix} 0 & f(\boldsymbol{k}) & 0 & 0 \\ f^*(\boldsymbol{k}) & 0 & -J_\perp/2 & 0 \\ 0 & -J_\perp/2 & 0 & f(\boldsymbol{k}) \\ 0 & 0 & f^*(\boldsymbol{k}) & 0 \end{pmatrix},$$

$$\mathcal{D}_{\rm FM} = \begin{pmatrix} 3J/2 & 0 & 0 & 0 \\ 0 & (3J + J_\perp)/2 & 0 & 0 \\ 0 & 0 & (3J + J_\perp)/2 & 0 \\ 0 & 0 & 0 & 3J/2 \end{pmatrix}.$$

The spectrum contains four branches:

$$E^{\pm}_1 = \frac{3J}{2} \pm |f(\boldsymbol{k})|,$$

$$E^{\pm}_2 = \frac{3J + J_\perp}{2} \pm \frac{\sqrt{J_\perp^2 + 4|f(\boldsymbol{k})|^2}}{2},$$

where $|f(\boldsymbol{k})|$ is linear in k near the Dirac points K, K', and thus $E^{\pm}_1$ cross at $3J/2$ linearly [see Fig. 3(a)]. Meanwhile,

$$E^{+}_2 \sim \frac{3J}{2} + J_\perp + \frac{|f(\boldsymbol{k})|^2}{J_\perp},$$

$$E^{-}_2 \sim \frac{3J}{2} - \frac{|f(\boldsymbol{k})|^2}{J_\perp},$$

which are quadratic in k near the Dirac points.

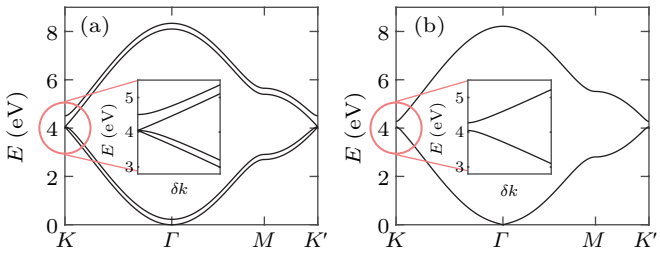


Fig. 3. The magnon bands along the high symmetric lines in the first Brillouin zone for AB-stacked bilayers with: (a) the interlayer FM coupling; (b) the interlayer AFM coupling. Insets of both figures show the enlarged plots of the magnon bands near the Dirac point.

Then we change interlayer coupling AFM. The bosonic tight binding Hamiltonian becomes

$$H^{\rm AB}_{\rm AFM} = -J_\perp \sum_i \frac{1}{2}(a^\dagger_{i_{\rm A},2} a^\dagger_{i_{\rm B},1} + a_{i_{\rm A},2} a_{i_{\rm B},1})$$

$$-\frac{J_\perp}{2}\sum_i (a^\dagger_{i_{\rm B},1}a_{i_{\rm B},1}+a^\dagger_{i_{\rm A},2}a_{i_{\rm A},2})$$
$$-J\sum_{\langle ij\rangle,\ell}\frac{1}{2}(a^\dagger_{i,\ell}a_{j,\ell}+a_{i,\ell}a^\dagger_{j,\ell})$$
$$+\frac{3J}{2}\sum_{i,\ell}a^\dagger_{i,\ell}a_{i,\ell}. \quad (11)$$

In the momentum space, we have

$$\mathcal{H}^{\rm AB}_{\rm AFM}(\boldsymbol{k})=\mathcal{H}^{\rm AB}_0(\boldsymbol{k})+\mathcal{D}_{\rm AFM}, \quad (12)$$

with

$$\mathcal{D}_{\rm AFM}=\begin{pmatrix} 3J/2 & 0 & 0 & 0\\ 0 & (3J-J_\perp)/2 & 0 & 0\\ 0 & 0 & (3J-J_\perp)/2 & 0\\ 0 & 0 & 0 & 3J/2\end{pmatrix}.$$

By diagonalizing $s_z\mathcal{H}^{\rm AB}_{\rm AFM}(\boldsymbol{k})$, we obtain the magnon spectrum

$$E^{\pm}_{\boldsymbol{k}}=\sqrt{\left(\frac{3J}{2}\right)^2\pm\frac{g(\boldsymbol{k})}{2}+|f(\boldsymbol{k})|^2-\left(\frac{3J}{2}\right)\frac{J_\perp}{2}},$$

with

$$g(\boldsymbol{k})=\sqrt{\frac{3J}{2}\left[\left(\frac{3J}{2}\right)J_\perp^2-8J_\perp|f(\boldsymbol{k})|^2+16\left(\frac{3J}{2}\right)|f(\boldsymbol{k})|^2\right]}.$$

Near the Dirac points,

$$E^+\sim\frac{3J}{2}+\frac{[4(3J/2)-J_\perp]|f(\boldsymbol{k})|^2}{2(3J/2)J_\perp},$$
$$E^-\sim\sqrt{\left(\frac{3J}{2}\right)^2-\left(\frac{3J}{2}\right)J_\perp}+\frac{[-4(3J/2)+3J_\perp]|f(\boldsymbol{k})|^2}{2J_\perp\sqrt{(3J/2)^2-(3J/2)J_\perp}},$$

which are quadratic in k. The spectrum is gapped on the Dirac points, with the gap size $3J/2-\sqrt{(3J/2)^2-(3J/2)J_\perp}$.

4. Twisted bilayer quantum magnets

By taking any vertical bond in AA-stacked bilayer as the axis, the twisted bilayers are generated by rotating one layer around the axis, while the other layer remains fixed. The periodicity is maintained for commensurate θ, when a certain site of one layer ends up exactly over a site of the other after the rotation. The Bravais lattice of the superstructure is hexagonal with the two unit vectors: $L_1=m\boldsymbol{a}_1+n\boldsymbol{a}_2$ and $L_2=-n\boldsymbol{a}_1+(m+n)\boldsymbol{a}_2$. Each supercell contains $N=4(m^2+mn+n^2)$ sites.[58,59] The twist angle writes as

$$\theta=2\sin^{-1}\frac{m-n}{2\sqrt{m^2+n^2+mn}}.$$

In the following, we consider the commensurate twist angles 21.8°, 6.01°, and 3.89°, which correspond to $(m,n)=(2,1),(6,5),(9,8)$, respectively. The case of smaller angles have too large supercells to deal with using our computer, and thus instead we calculate the magnon spectrum using the low-energy continuous theory near the Dirac points.[64,65]

The nearest-neighbor intralayer FM coupling are considered with the strength as the energy scale. The strength of interlayer coupling between sites r_i and r_j is given by $J_{ij}=J_\perp e^{-[(|r_i-r_i|-d_0)/\xi]}$, where the parameters are set as $J_\perp/J=-0.17$, $d_0=0.335$ nm, and $\xi=0.0453$ nm.

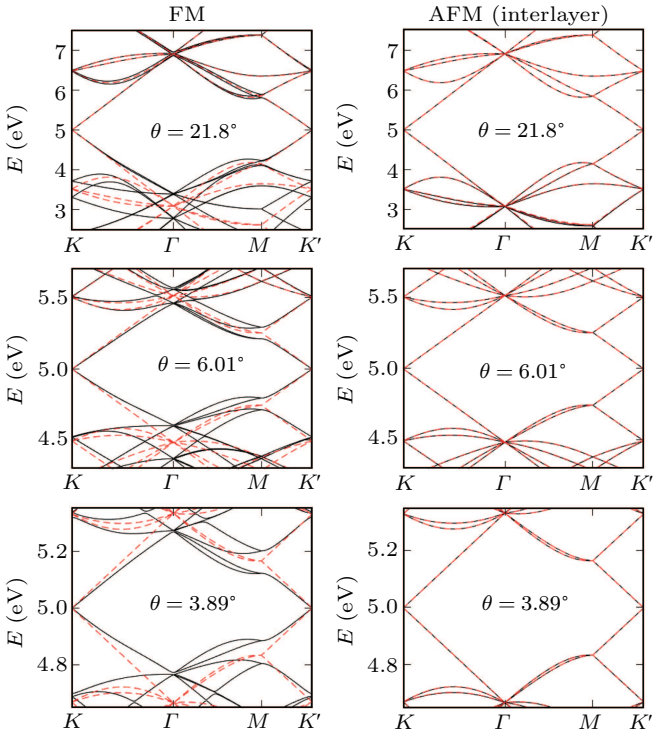


Fig. 4. Magnon band structures of twisted bilayers with twist angles of 21.8°, 6.01°, and 3.89°: (a)–(c) the interlayer FM coupling; (d)–(f) the interlayer AFM coupling. The intralayer couplings are FM case in all figures. We also plot the magnon spectrums without interlayer coupling (dashed red lines). To compare the Dirac velocity, the Dirac points are moved to the same positions as those in twisted bilayers.

The magnon spectrums are show in Fig. 4. Since the z component of each Heisenberg term generates a positive potential in the HP transformation, the bands are shifted upward compared to the cases without the interlayer coupling. The Dirac cones are preserved for

the studied angles. In the interlayer FM cases, while the slopes are almost unchanged for large twist angles ($\theta = 21.8^\circ, 6.01^\circ$), there is a clear reduction for small angle $\theta = 3.89^\circ$. The behavior is very similar to that of twisted bilayer graphene.[62,63] It is expected that the magnon bands becomes flatting as the angle is further decreased. In contrast, the spectrum of the interlay AFM case differs little from that of the single-layer quantum FM case, further verifying the spin excitations of opposite spin orientations do not couple with each other.

Now we begin to study the mangon spectrums of small twist angles using the low-energy continuous theory near the valley $\boldsymbol{K}_\pm = \left(4\pi/3\sqrt{3}a\right)(\pm 1, 0)$, where a is the lattice constant. Ignoring the overall potential from the z-component of the Heisenberg couplings, the effective bosonic Hamiltonian consists of three terms[64–71]

$$\begin{aligned} H_{\text{eff}}^{(\pm)} = \sum_{\boldsymbol{k}} \Big[& \psi_{\text{b}}^\dagger(\boldsymbol{k}) h_{\theta/2}^{(\pm)}\left(\boldsymbol{k} - \boldsymbol{K}_\pm^{\text{b}}\right) \psi_{\text{b}}(\boldsymbol{k}) \\ & + \psi_{\text{t}}^\dagger(\boldsymbol{k}) h_{-\theta/2}^{(\pm)}\left(\boldsymbol{k} - \boldsymbol{K}_\pm^{\text{t}}\right) \psi_{\text{t}}(\boldsymbol{k}) \\ & + \sum_{j=1}^{3} \left(\psi_{\text{b}}^\dagger(\boldsymbol{k}) T_j^{(\pm)} \psi_{\text{t}}(\boldsymbol{k} + \boldsymbol{X}_j^{(\pm)}) + \text{h.c.} \right) \Big] \end{aligned} \tag{13}$$

with $\boldsymbol{K}_\pm^t = \mathcal{R}_{\theta/2}\boldsymbol{K}_\pm$ and $\boldsymbol{K}_\pm^b = \mathcal{R}_{-\theta/2}\boldsymbol{K}_\pm$, where $\mathcal{R}_\theta$ rotates a vector by angle θ counterclockwise. $\boldsymbol{k}$ represents the momenta near the Dirac point $\boldsymbol{K}_\pm$, which writes as $\boldsymbol{k}_0 + m\boldsymbol{G}_1 + n\boldsymbol{G}_2 + \boldsymbol{Y}_\pm$ with $\boldsymbol{k}_0$ in the moiré first Brillouin zone and $\boldsymbol{Y}_\pm = (\boldsymbol{K}_\pm^t + \boldsymbol{K}_\pm^b)/2 \pm \boldsymbol{G}_1/2$. Here, $\boldsymbol{G}_1 = K_\theta(1, 0)$ and $\boldsymbol{G}_2 = K_\theta(-1/2, \sqrt{3}/2)$ with $K_\theta = [8\pi \sin(\theta/2)]/3a$ is the length of the basis vectors in the moiré Brillouin zone. In practice, the integers m, n are cut off to finite values, *i.e.*, $m, n = -l, \ldots, l$, and the magnon spectrums converge quickly as the cutoff value l increases. The first two terms describe the isolated FM sheets of the top and bottom layers under the bases

$$\psi_{\text{b}}(\boldsymbol{k}) = \begin{bmatrix} \varphi_{\text{A,b}}(\boldsymbol{k}) \\ \varphi_{\text{B,b}}(\boldsymbol{k}) \end{bmatrix}, \quad \psi_{\text{t}}(\boldsymbol{k}) = \begin{bmatrix} \varphi_{\text{A,t}}(\boldsymbol{k}) \\ \varphi_{\text{B,t}}(\boldsymbol{k}) \end{bmatrix}. \tag{14}$$

The low-energy Hamiltonian for a layer rotated by an angle θ is $h_\theta^{(\pm)}(\boldsymbol{k}) = \hbar v_{\text{f}}(\mathcal{R}_\theta \boldsymbol{k}) \cdot (\pm\sigma_x, \sigma_y)$, which is a Dirac one. The last term in Eq. (13) describes hoppings between layers with the hopping matrix

$$T_j^{(\pm)} = \omega \begin{bmatrix} 1 & \text{e}^{\mp 2\pi \text{i}/3(j-1)} \\ \text{e}^{\pm 2\pi \text{i}/3(j-1)} & 1 \end{bmatrix}, \tag{15}$$

and $\boldsymbol{X}_1^{(\pm)} = (0, 0)$, $\boldsymbol{X}_2^{(\pm)} = \pm(\boldsymbol{G}_1 + \boldsymbol{G}_2)$, and $\boldsymbol{X}_3^{(\pm)} = \pm\boldsymbol{G}_2$. The magnon spectrum is calculated directly, and the result for the $\theta = 3.89^\circ$ case is shown in Fig. 5. We find the interlayer coupling strength $\omega = 0.0439$ eV gives the best match between the continuous theory and exact tight-binding calculation. It is expected that ω will change with the twisted angle θ. However the determined strength at relatively large θ provides a good approximation for the cases of smaller angles, which are very hard to access in the tight-binding method.

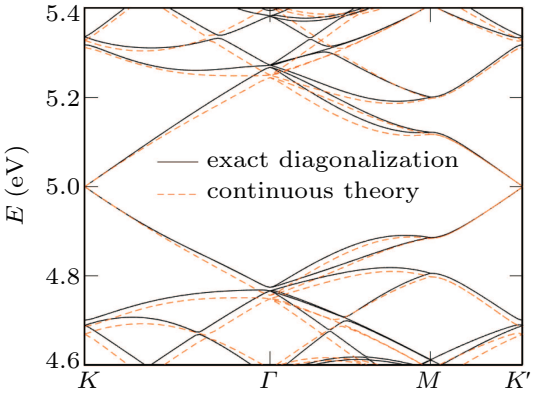


Fig. 5. Comparison of the low-energy magnon bands between the continuous theory and exact tight-binding calculation with the FM interlayer coupling. Here the twist angle is $\theta = 3.89^\circ$.

5. Conclusions

The magnon bands of both the bilayer and twisted bilayer honeycomb quantum magnets are studied using linear spin wave theory. The interlayer ferromagnetic order but two kinds of intralayer exchange couplings are considered. When the two layers are ferromagnetically coupled, the linear dispersions near the magnon Dirac points are preserved, and their slopes are reduced with the decrease of the twist angles. For the interlayer antiferromagnetic case, we find that the two monolayer magnon dispersions are usually decoupled due to the opposite orientations of the spins in the two layers. Finally a low-energy continuous theory is developed for the small twist angles, and fits well with the exact tight-binding calculations.

Experimentally there have revealed intrinsic magnetism in various atomically thin crystals. Among them, CrX_3 (X = Cl, Br, I) is a family of 2D honeycomb quantum magnets. Specifically, intralayer ferromagnetism and interlayer antiferromagnetism has been observed in bilayer CrI_3.[72–75] Besides, it has been proposed that the interlayer exchange coupling can be tuned between AFM and FM by changing the interlayer stacking order.[76] Thus based on these bilayer honeycomb quantum magnets, our results may be experimentally observed using

the state of the art measurements, such as inelastic neutron scattering and magneto-Raman spectroscopy.[77]

References

[1] Cao Y, Fatemi V, Demir A, Fang S, Tomarken S L, Luo J Y, Sanchez-Yamagishi J D, Watanabe K, Taniguchi T, Kaxiras E, Ashoori R C and Jarillo-Herrero P 2018 *Nature* **556** 80

[2] Xie M and MacDonald A H 2020 *Phys. Rev. Lett.* **124** 097601

[3] Saito Y, Ge J, Watanabe K, Taniguchi T and Young A F 2020 *Nat. Phys.* **16** 926

[4] Yankowitz M, Chen S, Polshyn H, Zhang Y, Watanabe K, Taniguchi T, Graf D, Young A F and Dean C R 2019 *Science* **363** 1745

[5] Cao Y, Fatemi V, Fang S, Watanabe K, Taniguchi T, Kaxiras E and Jarillo-Herrero P 2018 *Nature* **556** 1059

[6] Roy B and Juričić V 2019 *Phys. Rev. B* **99** 121407(R)

[7] Wu X, Hanke W, Fink M, Klett M and Thomale R 2020 *Phys. Rev. B* **101** 121407

[8] Liu C, Zhang L, Chen W and Yang F 2018 *Phys. Rev. Lett.* **121** 217001

[9] Balents L, Dean C R, Efetov D K and Young A F 2020 *Nat. Phys.* **16** 134517

[10] Chen G, Sharpe A L, Gallagher P, Rosen I T, Fox E J, Jiang L, Lyu B, Li H, Watanabe K, Taniguchi T, Jung J, Shi Z, Goldhaber-Gordon D, Zhang Y and Wang F 2019 *Nature* **572** 215

[11] Li X, Wu F and MacDonald A H 2019 arXiv preprint arXiv: 1907.12338

[12] Chen G, Jiang L, Wu S, Lyu B, Li H, Chittari B L, Watanabe K, Taniguchi T, Shi Z, Jung J, Zhang Y and Wang F 2019 *Nat. Phys.* **15** 237

[13] Shi Y, Xu S, Ezzi M M A, Balakrishnan N, Garcia-Ruiz A, Tsim B, Mullan C, Barrier J, Xin N, Piot B A, Taniguchi T, Watanabe K, Carvalho A, Mishchenko A, Geim A K, Fal'ko V I, Adam S, Neto A H C and Novoselov K S 2020 arXiv preprint arXiv: 2004.12414

[14] Wang L, Shih E, Ghiotto A, Xian L, Rhodes D A, Tan C, Claassen M, Kennes D M, Bai Y, Kim B, Watanabe K, Taniguchi T, Zhu X, Hone J, Rubio A, Pasupathy A and Dean C R 2020 *Nat. Mater.* **19** 215

[15] An L, Cai X, Pei D, Huang M, Wu Z, Zhou Z, Lin J, Ying Z, Ye Z, Feng X, Gao R, Cacho C, Watson M, Chen Y and Wang N 2020 *Nanoscale Horiz.* **01** 1281

[16] Shen C, Chu Y, Wu Q, Li N, Wang S, Zhao Y, Tang J, Liu J, Tian J, Watanabe K, Taniguchi T, Yang R, Meng Z Y, Shi D, Yazyev O V and Zhang G 2020 *Nat. Phys.* **16** 237

[17] Burg G W, Zhu J, Taniguchi T, Watanabe K, MacDonald A H and Tutuc E 2019 *Phys. Rev. Lett.* **123** 197702

[18] Chebrolu N R, Chittari B L and Jung J 2019 *Phys. Rev. B* **99** 861

[19] Culchac F J, Del Grande G R R, Capaz R B, Chico L and Morell E S 2020 *Nanoscale* **12** 4790

[20] May-Mann J and Hughes T L 2020 *Phys. Rev. B* **101** 520

[21] Luo X and Zhang C 2020 arXiv preprint arXiv: 2008.01351

[22] González-Tudela A and Cirac J I 2019 *Phys. Rev. A* **100** 053604

[23] Park J 2016 *J. Phys.: Condens. Matter* **28** 075109

[24] Burch K S, Mandrus D and Park J 2018 *Nature* **563** 47

[25] Gibertini M, Koperski M, Morpurgo A and Novoselov K 2019 *Nat. Nanotechnol.* **14** 180506

[26] Luo Z, Tang J, Ma B, Zhang Z, Jin Q and Wang J 2012 *Chin. Phys. Lett.* **29** 127501

[27] Tang J, Ma B, Zhang Z and Jin Q 2010 *Chin. Phys. Lett.* **27** 077502

[28] Sharpe A L, Fox E J, Barnard A W, Finney J, Watanabe K, Taniguchi T, Kastner M A and Goldhaber-Gordon D 2019 *Science* **365** 605

[29] Bultinck N, Chatterjee S and Zaletel M P 2020 *Phys. Rev. Lett.* **124** 166601

[30] Seo K, Kotov V N and Uchoa B 2019 *Phys. Rev. Lett.* **122** 5014

[31] Wu F and Das Sarma S S 2020 *Phys. Rev. B* **101** 245126

[32] Alavirad Y and Sau J 2020 *Phys. Rev. B* **102** 235123

[33] Thomson A, Chatterjee S, Sachdev S and Scheurer M S 2018 *Phys. Rev. B* **98** 075109

[34] Gu X, Chen C, Leaw J N, Laksono E, Pereira V M, Vignale G and Adam S 2020 *Phys. Rev. B* **101** 053604

[35] Huang T, Zhang L and Ma T 2019 *Sci. Bull.* **64** 310

[36] Zhang W, Wong P K J, Zhu R and Wee A T S 2019 *InfoMat* **1** 605

[37] Gao T, Zheng F, Wang X 2018 *Acta Phys. Sin.* **67** 167101 (in Chinese)

[38] Li H, Ruan S and Zeng Y 2019 *Adv. Mater.* **31** 166601

[39] Wang M, Huang C, Cheung C, Chen C, Tan S G, Huang T, Zhao Y, Zhao Y, Wu G, Feng Y, Wu H and Chang C 2020 *Annalen der Physik* **532** 1900452

[40] Ningrum V P, Liu B, Wang W, Yin Y, Cao Y, Zha C, Xie H, Jiang X, Sun Y, Qin S, Chen X, Qin T, Zhu C, Wang L and Huang W 2020 *Research* **2020** 1768918

[41] Ahn E C 2020 *npj 2D Mater. Appl.* **4** 17

[42] Novoselov K, Mishchenko A, Carvalho A and Neto A C 2016 *Science* **353** Issu 6298

[43] Sun Y, Tong W and Luo X 2019 *Phys. Chem. Chem. Phys.* **21** 24852

[44] Liu Y and Petrovic C 2017 *Phys. Rev. B* **96** 054406

[45] Liu Y and Petrovic C 2018 *Phys. Rev. B* **97** 014420

[46] Kim H H, Yang B, Li S, Jiang S, Jin C, Tao Z, Nichols G, Sfigakis F, Zhong S, Li C, Tian S, Cory D G, Miao G, Shan J, Mak K F, Lei H, Sun K, Zhao L and Tsen A W 2019 *Proc. Nat. Acad. Sci. USA* **116** 11131

[47] Wu Z, Yu J and Yuan S 2019 *Phys. Chem. Chem. Phys.* **21** 155149

[48] Zheng H, Yang B, Wang D, Han R, Du X and Yan Y 2014 *Appl. Phys. Lett.* **104** 132403

[49] Zhang W, Guo H T, Jiang J, Tao Q C, Song X J, Li H and Huang J 2016 *J. Appl. Phys.* **120** 235123

[50] Huang B, Clark G, Klein D R, MacNeill D, Navarro-Moratalla E, Seyler K L, Wilson N, McGuire M A, Cobden D H, Xiao D and others 2018 *Nat. Nanotechnol.* **13** 544

[51] Yang B, Zhang X, Yang H, Han X and Yan Y 2019 *Appl. Phys. Lett.* **114** 192405

[52] Onsager L 1944 *Phys. Rev.* **65** 117

[53] Mermin N D and Wagner H 1966 *Phys. Rev. Lett.* **17** 25220

[54] Kosterlitz J M and Thouless D J 1973 *J. Phys. C: Solid State Phys.* **6** 7750

[55] Balents L 2010 *Nature* **464** 132403

[56] Chang C, Zhang J, Feng X, Shen J, Zhang Z, Guo M, Li K, Ou Y, Wei P, Wang L and others 2013 *Science* **340** 013904

[57] Lee K H, Chung S B, Park K and Park J 2018 *Phys. Rev. B* **97** 180401(R)

[58] Rozhkov A V, Sboychakov A O, Rakhmanov A L and Nori F 2016 *Phys. Rep.* **648** 1–104

[59] Li S, Liu K, Yin L, Wang W, Yan W, Yang X, Yang J, Liu H, Jiang H and He L 2017 *Phys. Rev. B* **96** 155416
[60] Bistritzer R and MacDonald A H 2011 *Proc. Nat. Acad. Sci. USA* **108** 12233
[61] Lopes dos Santos d S J M B, Peres N M R and Castro Neto N A H 2012 *Phys. Rev. B* **86** 4155449
[62] Suárez Morell M E, Correa J D, Vargas P, Pacheco M and Barticevic Z 2010 *Phys. Rev. B* **82** 121407(R)
[63] Trambly de Laissardire d L G, Mayou D and Magaud L 2010 *Nano Lett.* **10** 054406
[64] Bistritzer R and MacDonald A H 2011 *Proc. Nat. Acad. Sci. USA* **108** 12233
[65] Lopes dos Santos d S J M B, Peres N M R and Castro Neto N A H 2012 *Phys. Rev. B* **86** 014420
[66] Koshino M 2015 *New J. Phys.* **17** 015014
[67] Koshino M, Yuan N F Q, Koretsune T, Ochi M, Kuroki K and Fu L 2018 *Phys. Rev. X* **8** 11131
[68] Lee J Y, Khalaf E, Liu S, Liu X, Hao Z, Kim P and Vishwanath A 2019 *Nat. Commun.* **10** 544
[69] Ma Z, Li S, Zheng Y, Xiao M, Jiang H, Gao J and Xie X 2021 *Sci. Bull.* **66** 192405
[70] Abouelkomsan A, Liu Z and Bergholtz E J 2020 *Phys. Rev. Lett.* **124** 106803
[71] Balents L 2019 *SciPost Physics* **7** 048
[72] Huang B, Clark G, Navarro-Moratalla E, Klein D R, Cheng R, Seyler K L, Zhong D, Schmidgall E, McGuire M A, Cobden D H and others 2017 *Nature* **546** 1133
[73] Song T, Cai X, Tu M W, Zhang X, Huang B, Wilson N P, Seyler K L, Zhu L, Taniguchi T, Watan K, McGuire M A, Cobden D H, Xiao D, Yao W and Xu X 2018 *Science* **360** 1214
[74] Klein D R, MacNeill D, Lado J L, Soriano D, Navarro-Moratalla E, Watanabe K, Taniguchi T, Manni S, Canfield P, Fernández-Rossier J and Jarillo-Herrero P 2018 *Science* **360** 1181
[75] Thiel L, Wang Z, Tschudin M A, Rohner D, Gutiérrez-Lezama I, Ubrig N, Gibertini M, Giannini E, Morpurgo A F and Maletinsky P 2019 *Science* **364** 199
[76] Sivadas N, Okamoto S, Xu X, Fennie C J and Xiao D 2018 *Nano Lett.* **18** 167
[77] Cenker J, Huang B, Suri N, Thijssen P, Miller A, Song T, Taniguchi T, Watanabe K, McGuire M A, Xiao D and others 2020 *Nat. Phys.* **17** 20